

CIRCULATION COPY
SUBJECT TO RECALL
IN TWO WEEKS

UCRL- 91490
PREPRINT

THE MOTION OF THIN METAL WALLS AND THE EQUATION
OF STATE OF DETONATION PRODUCTS

E. Lee, D. Breithaupt,
C. McMillan, N. Parker,
J. Kury, C. Tarver,
W. Quirk, and J. Walton

This paper was prepared for submittal to:
8th Symposium (International) on
Detonation, July 15-19, 1985
Albuquerque, NM

July 8, 1985

Lawrence
Livermore
National
Laboratory

This is a preprint of a paper intended for publication in a journal or proceedings. Since changes may be made before publication, this preprint is made available with the understanding that it will not be cited or reproduced without the permission of the author.

DISCLAIMER

This document was prepared as an account of work sponsored by an agency of the United States Government. Neither the United States Government nor the University of California nor any of their employees, makes any warranty, express or implied, or assumes any legal liability or responsibility for the accuracy, completeness, or usefulness of any information, apparatus, product, or process disclosed, or represents that its use would not infringe privately owned rights. Reference herein to any specific commercial products, process, or service by trade name, trademark, manufacturer, or otherwise, does not necessarily constitute or imply its endorsement, recommendation, or favoring by the United States Government or the University of California. The views and opinions of authors expressed herein do not necessarily state or reflect those of the United States Government or the University of California, and shall not be used for advertising or product endorsement purposes.

THE MOTION OF THIN METAL WALLS AND THE EQUATION OF STATE OF DETONATION PRODUCTS

E. Lee, D. Breithaupt, C. McMillan, N. Parker, J. Kury,
C. Tarver, W. Quirk, and J. Walton
Lawrence Livermore National Laboratory
University of California
Livermore, CA 94550

In this paper we will report high resolution measurements we have made using cylinders and flat plates to determine detonation product behavior. By using thin walled cylinders and thin plates and by utilizing both streak camera and Fabry-Perot velocimeter techniques we can achieve resolution and accuracy much greater than previously attained. As an example we will present results for an explosive formulation, LX-14, containing 95% HMX and 5% polyurethane and compare these experimental results with the results of hydrodynamic calculations carried out with accuracy equivalent to our experiment uncertainty. By using very thin plates and by varying plate thickness we are largely able to derive the explosive behavior independent of the metal properties. The reaction zone in the explosive can be resolved in the acceleration of the thinnest plates. This reaction front behavior is taken into account in the equation of state description. We show that the cylinder test measurements sample the EOS at expansion ratios $V/V_0 > 1$. Thin flat plates aligned in the plane of the detonation front provide detailed information on the higher compression states ($V_{CJ} < V/V_0 < 1.3$). Our results generally confirm the results of earlier work with respect to the pressure derivatives. The results require that $(\partial \ln P / \partial \ln V)_S$ increase as the products expand from the C-J state.

INTRODUCTION

The magnitudes of the pressures and temperatures encountered in condensed explosives during detonation are far beyond the capabilities of static pressure measurement techniques. Since the discovery of detonation, equations of state of explosive detonation products have been derived from dynamic measurements. Some of the earliest work⁽¹⁾ utilized the detonation velocity dependence on loading density. Methods used to the present day, first developed extensively by Walsh,⁽²⁾ and Deal⁽³⁾, utilize witness materials to determine pressure and volume from shock impedance relations at the explosive material interface. The work presented here follows our previous work⁽⁴⁾ which relies on hydrodynamic analysis of the history of the outer surface of an explosive charge as defined by a metal wall.

In earlier work our principal diagnostic was the rotating mirror streak camera (RMC) which measured the progress of cylinder expansion by observing the motion of the shadow of an intensely back-lighted cylinder moving across a narrow slit. Others⁽⁵⁾ have successfully used pin arrays and inclined prism techniques. The cylinder expansion measurements are limited since they effectively span the EOS for expansion ratios > 1.0 . Measurements at the detonation head i.e., normal to the detonation front have

been limited by experimental capabilities. The current work has taken advantage of recent developments in laser diagnostic techniques⁽⁶⁾ for both cylinder (lateral) and plane wave (head-on) measurements of witness plate motion.

We have also refined the slit measurement techniques applied to the cylinder expansion experiments. The comparison of the two techniques has provided valuable assurance for the precision and accuracy of the measurements.

At the same time the increased size and speed of computers has now allowed us to obtain calculations comparable to our experimental resolution in both the plane wave and cylinder configurations. In addition we are able to implement more detailed models to describe the detonation process and the response of witness materials.

To illustrate this approach to deriving EOS from dynamic measurements we will present results on a pressed plastic bonded explosive, LX-14, which is formulated using 5% by weight polyurethane and 95% HMX.

*Work performed under the auspices of the U.S. Department of Energy by the Lawrence Livermore National Laboratory under contract No. W-7405-ENG-48.

The hydrodynamic analysis of the experiments requires a description for the equation of state. Of the various algebraic forms we have utilized to represent the EOS, the JWL or an extended JWL has proven to be useful for this study. The form provides a flexible description and provides the ability to calculate results for pressure and energy in analytic form. The important results are derived from comparisons of experiments and calculations. These comparisons reveal the precision to which one can determine the equation of state of the detonation products. To this end the results are independent of the form of the EOS.

EXPERIMENTAL METHODS

The Explosive Material

For these tests we used a coarse grained LX-14 and a fine grained LX-14. The coarse grained material contains HMX particles as large as 400 μ , the fine grained contains HMX particles no larger than 40 μ . Parts were pressed to 98.30 \pm 3 percent of theoretical density for both materials. For the cylinder test we used only the coarse grained LX-14.

Cylinder Test

The configuration for the cylinder test has been modified for the work described here as shown in Fig. 1. Important features which differ from earlier work⁽⁴⁾ are that a large plane wave booster is used to provide an initiation source which is as flat and as nearly normal to the tube axis as possible. The pin rings, one near each end of the cylinder are used to determine detonation velocity but are also indexed so as to measure any tilt in the detonation wave. Two rotating mirror streak cameras (RMC's) are used one of which operates at higher streak speeds to better resolve the early motion. The principal modification is of course the use of Fabry-Perot interferometers (FPI). In fact two FPI's are arranged to monitor opposite sides of the cylinder near the slit level of the streak camera.

In the current experiments we use a 2" copper cylinder machined with a .100" copper wall. In earlier work we used 1" tubes with .100" wall. The current geometry provides twice the resolution in monitoring the pressure change in the "fluid."

Front Surface Plates

A diagram of the plane wave test configuration is shown in Fig. 2. The diagram illustrates several configurations all of which have been used to obtain plate velocity records. We have indicated in the diagram the range of plate thicknesses, explosive thickness, and initiating systems used for these experiments. Our calculations have taken into

account the variations in initiation mode (rear surface conditions). The majority of the tests used a mylar flyer which provides an extremely prompt initiation and flat wave profile.

RESULTS AND ANALYSIS

Cylinder Test

The analysis of cylinder tests based on rotating mirror camera (RMC) slit measurements is relatively straightforward. A computer program was developed to reduce Lagrangian hydrocode results for comparison with the laboratory slit reference plane.

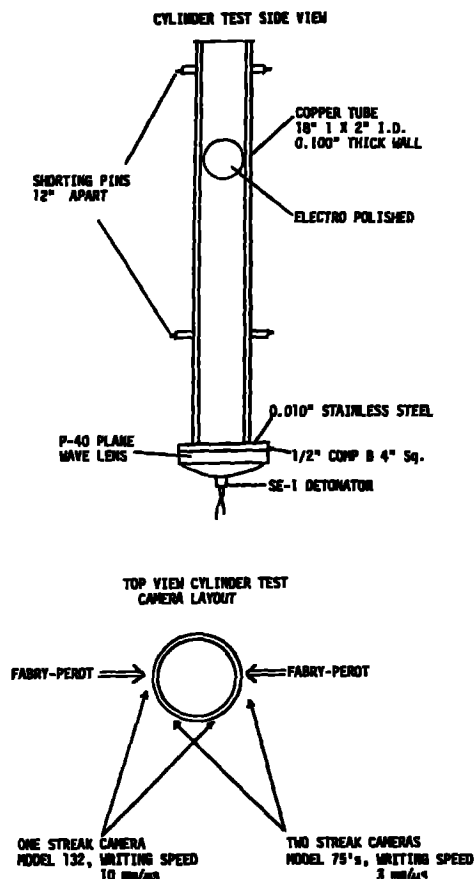


Fig. 1 Configuration for the cylinder test.

In order to compare the cylinder test data from the Fabry-Perot velocimeter with the radius/time data taken from the rotating mirror streaking camera (RMC), it is necessary to make two adjustments, one in amplitude, the other in time. These adjustments are needed because the Fabry-Perot and the RMC are actually measuring two very different quantities. The RMC measures what might be called an "obscuraton rate."

velocity can be written

$$V_S = V_d \tan \theta_S$$

where V_S is the velocity as measured along the slit of the RMC, V_d is the detonation velocity of the HE, and θ_S is the local angle of the cylinder surface relative to the unperturbed surface. The Fabry-Perot measures the particle velocity scaled by the dot product of the particle direction and the laser beam direction. This can be written

$$V_{fp} = V_p \cos(\theta_p - \theta_a)$$

where V_{fp} is the velocity as measured by the Fabry-Perot, V_p is the magnitude of the particle velocity, θ_p and θ_a are the angles formed by the particle trajectory and the laser with the original normal to the cylinder surface.

θ_S and \hat{V}_p are related through the hydrodynamics of the cylinder shot. Two simplifying assumptions make it possible to generate an analytical relation between them. First, that the flow is self similar, second, that the particle trajectories are adequately approximated by straight lines. The second, assumption is supported by hydrodynamic code calculations. From these assumptions, a relation between V_S and V_{fp} can be generated of the form

$$V_S(t) = A V_{fp}(t + \Delta t)$$

where

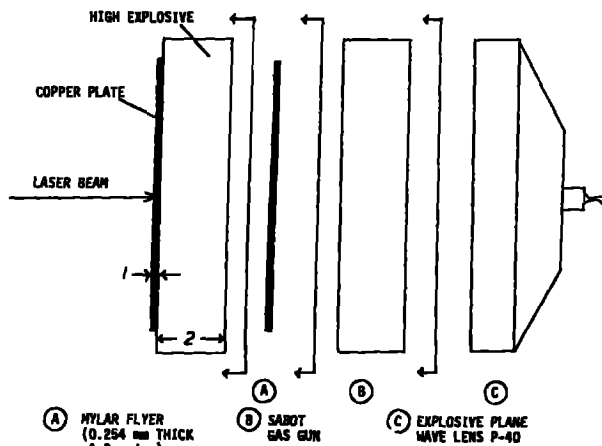
$$A = \left[\frac{\cos(\theta_p - \theta_L)}{\cos \theta_p} - V_{fp}(t + \Delta t) \frac{\tan \theta_p}{V_d} \right]^{-1},$$

$$\Delta t = r(t) \tan \theta_L / V_d,$$

and

$$r(t) = \int_0^t V_S(\tau) d\tau.$$

This relation has been tested by using a hydro code to calculate both the Fabry-Perot record and the record that would be seen by the RMC. A comparison these records based on this algorithm is shown in Fig. 4. In this figure the transform described here is compared with the slit and particle velocity edits from a single [thus-self consistent] hydrodynamic calculation. The transform, C, is shown to be identical to the hydrodynamic code results, A.



Legend (1) copper .001" .005", .010" 0.20", .100" nominal thickness, (2) HE 10, 20, 40, 100 mm

Fig. 2 A diagram of the plane wave test configuration.

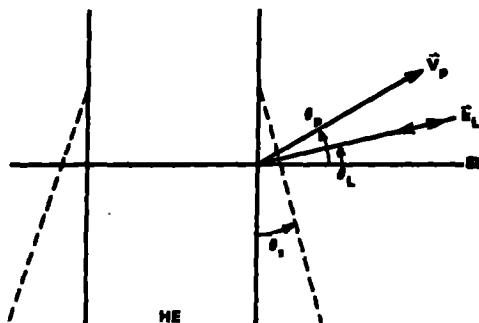


Fig. 3 Vector diagram of cylinder test wall motion.

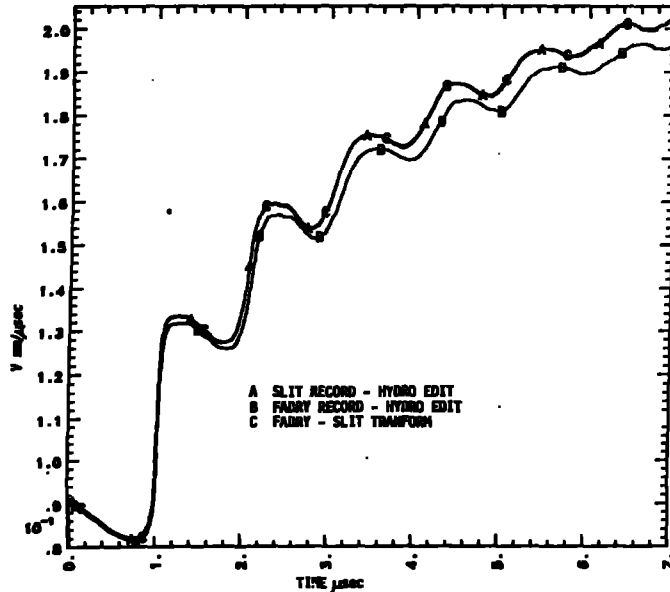


Fig. 4 Transform of Fabry Perot velocities to RMC velocities.

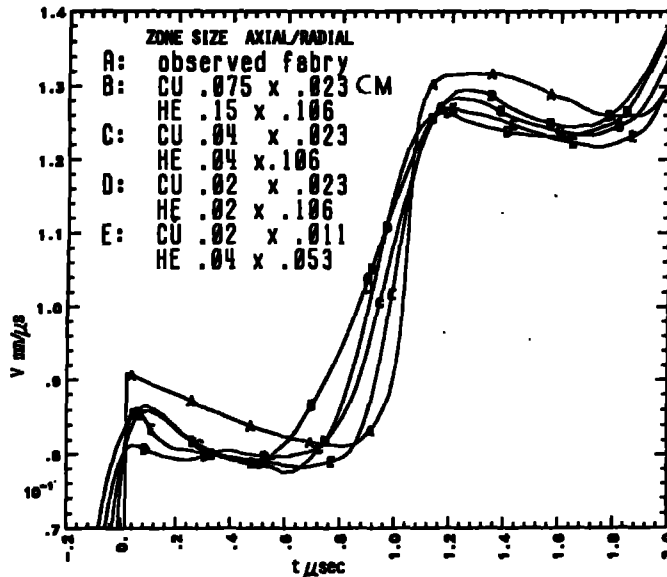


Fig. 5 Zoning study for cylinder test initial motion.

In Fig. 5 we show the results from a zoning study which examined the calculational resolution required to be equivalent to the experimental results. In this example the measured velocities were not matched, the object being to compare the time resolution. The resulting calculational model parameters labelled E which matched the experimental resolution were used in subsequent analysis.

In Fig. 6 we have shown the sensitivity of the calculational results to changes in the equation of state. The CJ parameters and coefficients for the various EOS's used in these comparisons are given in Table 1. The copper EOS is listed in Table 2.

Figure 6a shows clearly that the cylinder test is insensitive to the magnitude of the Chapman Jouguet pressure. The calculations compare EOS's which give P_{CJ} 's of .370 and .336 Mbar respectively, both of which match the cylinder test data. Nevertheless the test is sensitive to EOS differences at larger expansion ($V/V_0 > 1.1$) as shown in Fig. 6b. The differences in pressure for the EOS's in Fig. 6b are less than 2% at equal expansion in the range $1.0 < V < 3.0$. The pressure and energy differences are illustrated in Fig. 7a and 7b. The relation between cylinder test results and EOS results is based on the simple geometric relation R - internal tube radius

$$(R/R_0)^2 = (V/V_0)$$

Table 1
CJ Parameters and Equation of State Coefficients

Label	370A	370B	360A	336A	370T	
Parameters						
P	.370	.370	.360	.336	.370	mb
P_0	1.835	1.835	1.835	1.835	1.835	g/cm^{-3}
D	.880	.880	.880	.883	.880	on. μs
E_0	.102	.102	.102	.088	.1005	mb
Γ	2.84	2.84	2.947	3.258	2.84	
Coefficients						
A	8.261	8.677	11.65	129.46	-0-	
B	.1724	.2765	.5572	1.693	-0-	
C	.01296	.02604	.01844	.00183	.1303	
R_1	4.55	4.8	5.4	9.96	4.	
R_2	1.32	1.7	2.0	2.5	2.	
ω	.38	.6	.45	.1	1.84	

$$P = A(1 - \frac{\omega}{R_1 V})e^{-R_1 V} + B(1 - \frac{\omega}{R_2 V})e^{-R_2 V} + \frac{\omega E}{V} \quad V = \frac{V}{V_0}$$

Table 2
Copper Equation of State*

ρ_0	C	S_1	S_2	S_3	γ_0	a
8.93	.394	1.489	0.0	0.0	2.02	.47

* Gruneisen equation-of-state based on Hugoniot data.

$$U_s = C + S_1 U_p + S_2 U_p^2 + S_3 U_p^3$$

$$p = \frac{p_0 c^2 \mu [1 + (1 - \frac{\gamma_0}{2}) \mu - \frac{a}{2} \mu^2]}{[1 - (S_1 - 1) \mu - S_2 \frac{\mu^2}{2} - S_3 \frac{\mu^3}{(\mu+1)^2}]^2} + (\gamma_0 + a\mu)e$$

$$\mu = \frac{p}{p_0} - 1$$

We indicate in Fig. 8a, 8b and 8c the precision and reproducibility of the current cylinder test in this expansion range. These slit RMC and FPI measurements record the expansion over the range $V_{CJ} < V/V_0 < 2.1$. the experimental precision is comparable to the EOS comparisons in Fig. 6c. The overall estimated error for the velocities and displacements of $\frac{1}{2}\%$ corresponds to 1% in energy and pressure.

Front Surface Plates

The flat plate measurement using the Fabry-Perot is perfectly straightforward since the plate as shown in Fig. 2 is aligned perpendicular to the FPI beam. An interesting feature of these measurements is the trend of results as the plate thickness is varied as shown in Fig. 9a. By varying the EOS, particularly the value of the CJ pressure, the Fabry-Perot calculation results can be brought into agreement with the experimental results. The initial velocity of the plate is very nearly a direct measure of P_{CJ} in this study since the ratio $d_{plate}/d_{HE} \ll 1.0$ for all of the tests. However, the subsequent velocity steps depend upon the plate thickness and the EOS, as shown in Fig. 9.

A series of tests were performed on LX-14 in which the explosive thickness and the plate thickness were varied. The dimensional variations are given in Fig. 2. We have presented comparisons of experimental and calculational results in Table 3. The results show that an EOS which yields a $P_{CJ} = 360$ and which represented the early cylinder velocities also predicts the head on flat plate data to within the experimental error. We have no evidence of a lack of scaling except for the thinnest (.001", .025 mm) plates. The results also show that for plate thickness varying over the range .0010" - .100" and HE thickness of 10-100 mm the experimental results can be calculated to within the experimental accuracy $\pm 2\%$ with a single EOS. We have included an explanation of Table 3 in the form of a sample result shown in Fig. 10. the first four velocity increments and the velocity at the termination of the record are presented in the table along with comparisons to a standard calculation based on eos360A. The comparison for V_L is appropriate to the time t_L last for that particular experimental test.

Based on calculations which include realistic reaction zone behavior in the front we do not expect the thicker plates to be affected by von Neumann spike behavior. Results on extremely thin copper plates (.025 mm) compared to plates 10x thicker clearly indicate the regime where "von Neumann spike" effects become important. Experimental results and reactive flow model results⁽⁷⁾ are compared in Fig. 11.

The precision of the EOS description is determined by comparing calculated results for specific variations in the Equations of State. For a variation in energy δE or in pressure δP we can, in a particular region of expansion, in the cylinder test, determine the variations in velocity, δV , or displacement, δX , which fall within experimental error and thus determine the precision of the EOS. The internal energy change on expansion of the detonation products is very nearly proportional to the kinetic energy of the witness plate in the case of the cylinder test.

For front surface plate tests the initial velocity is directly related to the detonation front pressure. In fact, free surface velocity measurements on metal plates have commonly been used to determine detonation front pressures^(8,9).

At the copper/explosive interface the reflected detonation shock pressures far exceed C-J pressure. Nevertheless the initial free surface of a copper plate is determined by the "C-J" pressure. Variations in the compression and expansion regime of the EOS have a negligible effect on the initial velocity. To illustrate this point, a comparison of calculated velocities using, as shown in Fig. 12, two very different equations of state, I-law, and JWL, both yielding a P_{CJ} of 370 kb. A comparison of the calculated pressures is shown in Fig. 7b.

The resolution of the Fabry-Perot measurements allow us to examine this initial motion and the subsequent motion in detail. In the course of our experiments, as we increased the resolution of the measurements, we found that the initial velocities varied by as much as 10% between experiments. We attribute this to the heterogeneity in our standard LX-14. On one test of coarse grained material using a .020" plate shown in Fig. 13 the profile of the initial velocity increment deviates from the hydrodynamic calculational prediction. The same experiment using fine grained material is in excellent agreement with the hydrodynamic model. We have observed similar deviations with thinner plates .010" even with fine grained material and with thick plates .100" using coarse material.

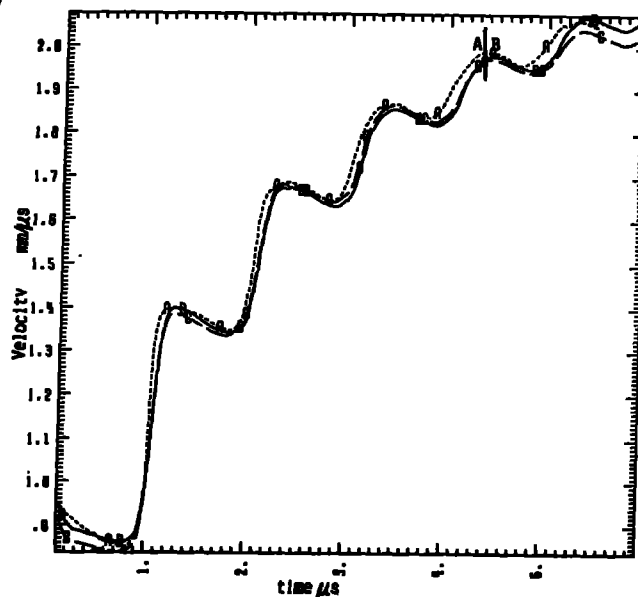
It seems clear that the accuracy of the plate test measurements is limited not by our ability to measure velocities but by our ability to reproduce the explosive/metal interface.

The succeeding velocity increments can only be interpreted by comparison with hydrocode results. As an extreme case, we have shown in Fig. (12) the difference between Γ law EOS and JWL EOS. Both EOS's yield a P_{CJ} of 370 kb but the expansion pressures for Γ law are considerably higher. The initial velocity increment is as we have pointed out, the same for both EOS's. However, the succeeding velocity increments differ roughly in proportion to the pressure difference in the region behind the plates.

CONCLUSION

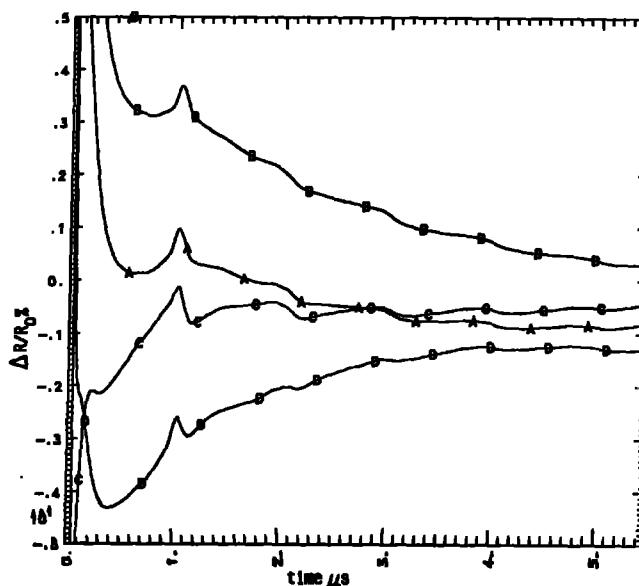
We have developed experimental tests and analysis procedures which produce an accurate determination of the detonation performance of explosives. In the course of the study we found it necessary to make improvements in experimental diagnostics and procedures and also in the calculational analysis. The results have provided a determination of early expansion to within 2% in velocity and pressure and at greater expansion to within 1/2% in velocity or 1% in energy and pressure. We believe the methods described in this work can be used to obtain precise descriptions for applied work and precise data for equation of state studies.

We have used the definition of P_{CJ} throughout as a convenient initial condition at the shock front. We have considered "von Neumann spike" phenomena and accounted for the effects. We have not treated or ruled out kinetic effects with longer time scales. An "effective" shock front pressure and particle velocity corresponding to $P_{CJ} = 360$ Mb are consistent with the details of the experimental results described here. If the products are treated as an equilibrium mixture of gases and condensed phases the expansion described here is the proper description. On this basis our results show that the isentropic index $\gamma = (\partial \ln P / \partial \ln V)_S$ must increase for increasing volume in the region of $V_{CJ} < V < 1.1$ in order to match the experimental data. We believe that a consistent treatment of longer time scale ($> 1 \mu s$) kinetic effects such as the formation of solid carbon near the detonation front may very well alter this description. At the present time, however, no such treatment exists.



Legend
 ... A. F.P.I. velocities averaged of test 520, 521
 — C Calculation based on $P_{CJ}=336$ JWL EOS
 — B Calculation based on $P_{CJ}=370$ JWL EOS

Fig. 6a Experimental and calculational cylinder test results for LX-14.



A $R(eos370A - FPI)/R(FPI)$
 B $R(eos370B - FPI)/R(FPI)$
 C $R(eos360A - FPI)/R(FPI)$
 D $R(eos336A - FPI)/F(FPI)$

Fig. 6b Comparison of calculational and experimental cylinder test results.

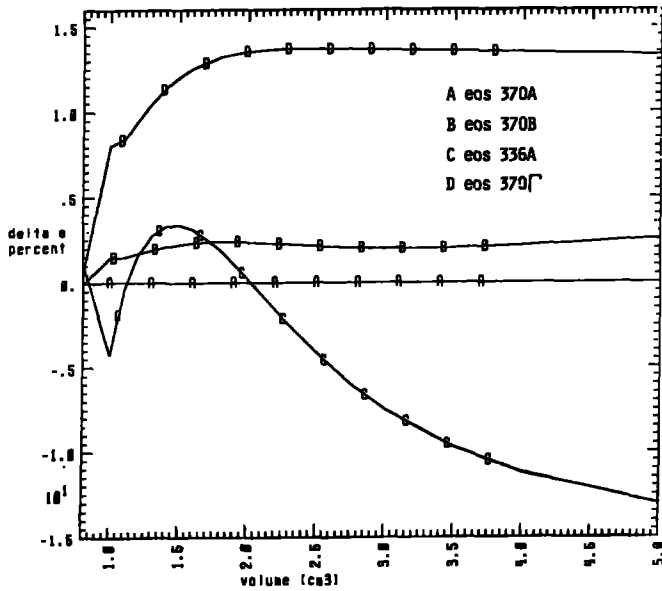
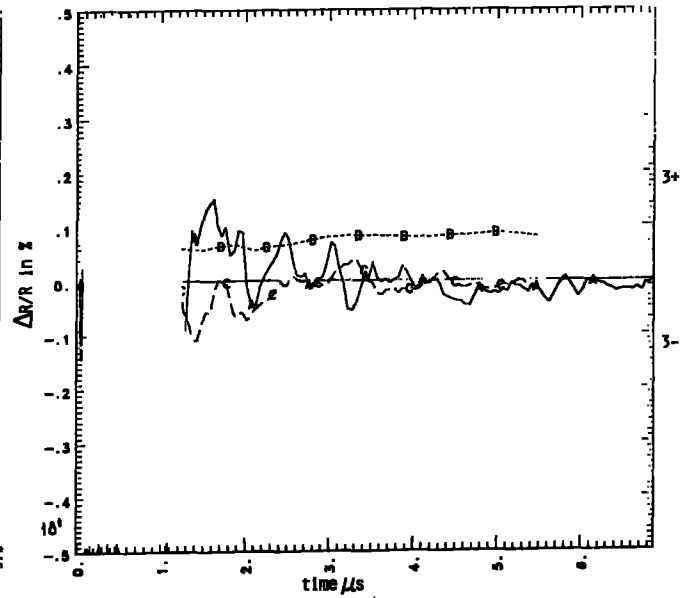


Fig. 7a Fractional internal energy change comparisons for various EOS's.

$$\delta E = \frac{(\Delta E \text{ EOS}(x) - \Delta E \text{ EOS } 370A)}{\Delta E \text{ EOS } 370A}$$



A % difference slit radii 521-520
B % difference Fabry radii 521-520
C % difference average radii slit-Fabry 520-521

Fig. 8 Comparison of deviations between experiments and test methods.

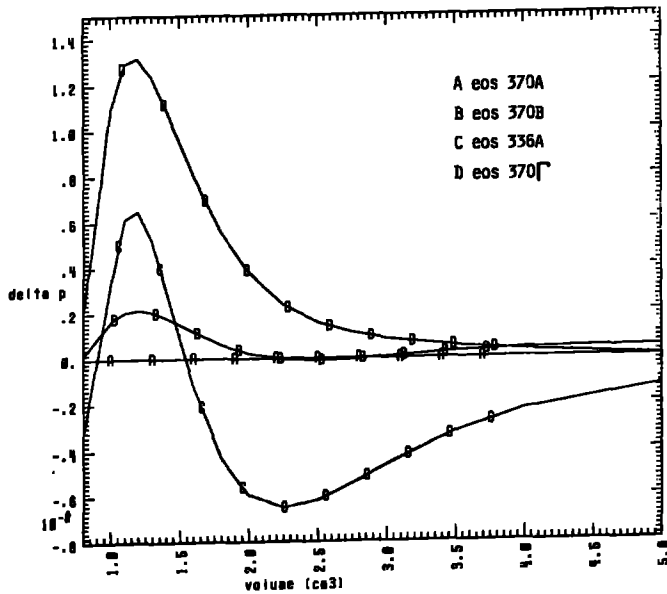


Fig. 7b Pressure comparisons for various EOS's.

$$\delta P = \frac{P \text{ EOS}(x) - P \text{ EOS } 370A}{P \text{ EOS } 370A}$$

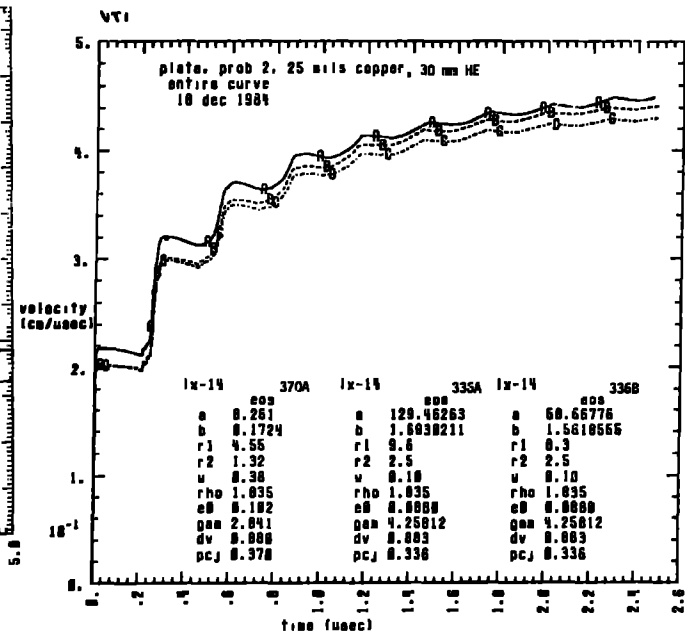


Fig. 9a Calculational results for a front surface copper plate d = .625 mm

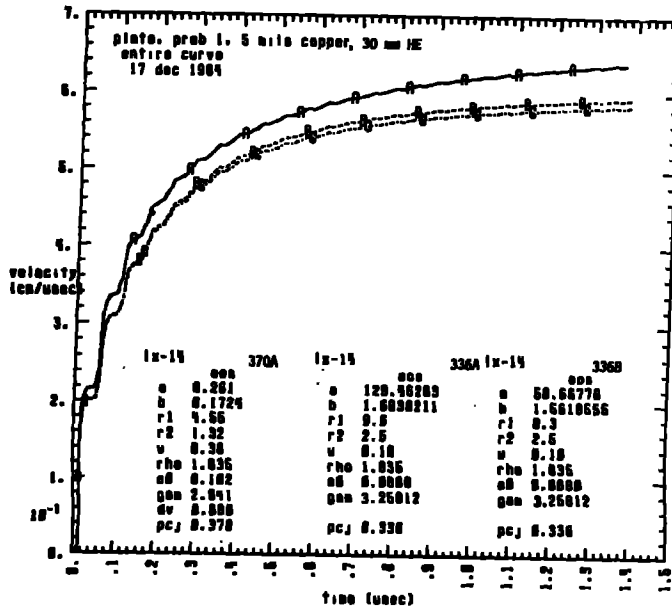
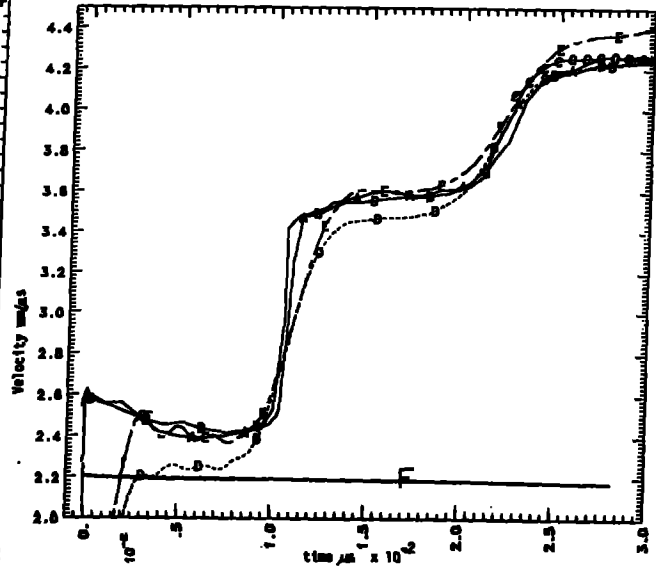


Fig. 9b Calculational results for a front surface copper plate $d = .125$ mm.



A,B,C - experimental records .001" Cu
D - standard burn model
E - reactive flow "von Neumann spike" calculation
F - experimental result .010" Cu

Fig. 11 Experimental and calculational results for .001" (.025 mm) Cu plate/25 mm LX-14.

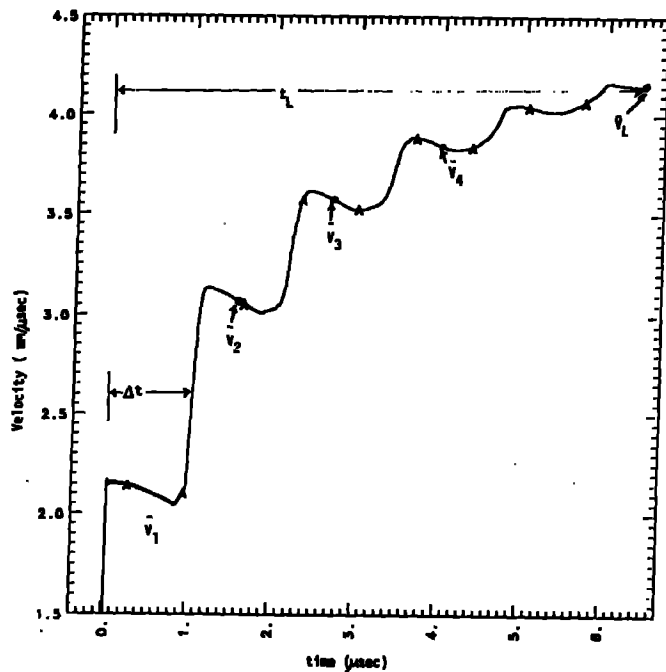
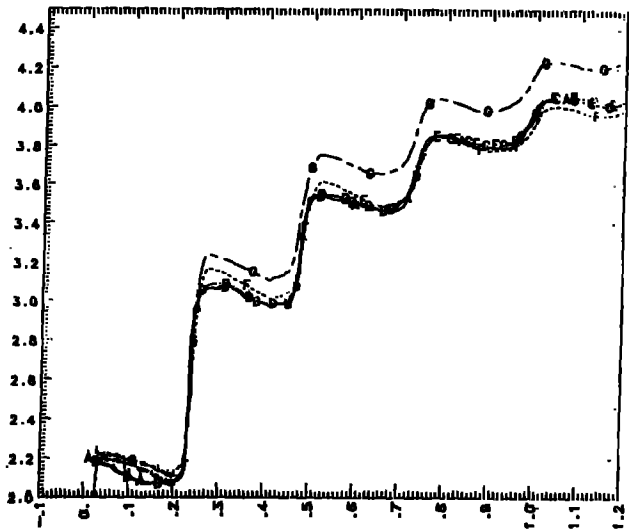


Fig. 10 Typical FPI results for front plate test. Example shown is for .100" (2.54 mm) Cu plate driven by 100 mm of explosive.



A,B,C,D,E - experimental FPI results
F - eos 370A
G - eos 370 I

Fig. 12 Comparison of experimental and calculational results for FPI measurements on .020" Cu plates/20 mm fine grained LX-14.

Table 3

SHOT	#9642	#9643	#9632	#9495	#9579	#9526	#9635	#9636
Copper Thickness (mm)	.0254			.123		.126	.257	
LX-14 Length (mm)	25.58			20.18		19.97	40.15 ^o	
X_{Cu}/X_{LX-14}	.0010			.0061		.0063	.0064	
$-At^a$ (μsec)	.01			.05		.05	.10	
V_1 (mm/μsec)	2.43 ^b (+10.5%)	2.49 (+13.5%)	2.63 (+19.5%)	2.10 (-2.5%)	-	2.20 (+2%)	2.24 (+3.5%)	2.05 (-5%)
V_2 (mm/μsec)	3.56 (+5%)	3.60 (+6%)	3.66 (+7.5%)	3.16 (-5%)	3.17 (-4.5%)	3.22 (-3%)	3.36 (+1.0%)	3.20 (-3.5%)
V_3 (mm/μsec)	4.24 (+2.5%)	4.22 (+2.5%)	4.28 (+3.5%)	3.85 (-4%)	3.83 (-4.5%)	3.83 (-4.5%)	4.00 (0%)	3.88 (-3.5%)
V_4 (mm/μsec)	4.68 (+1.5%)	4.64 (+5%)						
V_L (mm/μsec)	5.60 (-1.5%)	5.48 (-5%)				5.86 (0%)	5.50 (+2%)	5.37 (-5%)
t_L (μsec)	.08	.076				1.0	1.0	1.0

SHOT	#BP1	#BP2	#9578	#9577	#9634	#9633	#9527	#BP5	#BP6	#9528
Copper Thickness (mm)	2.502	2.520	.505		.526		.530	2.530	2.530	.532
LX-14 Length (mm)	101.61	101.60	20.15		19.95 ^(o)		20.00	92.02	91.07	10.01
X_{Cu}/X_{LX-14}	0.246	0.248	.0251		.0265		.0265	.0275	.0278	.0532
$-At^a$ (μsec)	1.00	1.00	.20		.20		.20	1.00	1.00	.20
V_1 (mm/μsec)	2.14 ^(b) (+1%)	2.17 (+2.5%)	2.02 (-4%)	2.22 (+6%)	2.12 (+1.5%)	2.12 (+1.5%)	2.11 (+1%)	2.11 (-5%)	2.15 (+1.5%)	2.03 (+1%)
V_2 (mm/μsec)	3.08 (+5%)	3.16 (+3%)	3.04 (-1%)	3.09 (+1%)	3.07 (+1%)	3.03 (-5%)	3.03 (-5%)	3.06 (+5%)	3.06 (+5%)	2.79 (+1%)
V_3 (mm/μsec)	3.60 (+1%)	3.67 (+3%)	3.62 (+2%)	3.60 (+1.5%)	3.55 (1%)	3.50 (-5%)	3.57 (+1.5%)	3.55 (+5%)	3.57 (+1%)	3.11 (+1.5%)
V_L (mm/μsec)			4.42 (+2%)	4.43 (+2%)	4.31 (+5%)	4.35 (+1.5%)	4.35 (+2%)			3.42 (+1%)
t_L (μsec)			2.0	2.0	2.0	2.0	2.0			1.4

Shot	#9586	#9587
Aluminum Thickness (mm)	.515	
LX-14 Length (mm)	20.23	
X_{Al}/X_{LX-14}	.0255	
$-At^a$ (μsec)	.17	
V_2 (mm/μsec)	4.79 (+1.5%)	4.65 (-1.5%)
V_3 (mm/μsec)	5.22 (+1.5%)	5.10 (-1%)
V_L (mm/μsec)	5.87 (+1%)	5.82 (0%)
t_L (μsec)	1.5	1.5

a See Fig. 10 for definition of t and V

b Numbers in () are differences of experimental velocities and those calculated with LX-14 EOS #360A.

c Special formulation with small particle size HMX

Lee, et al.

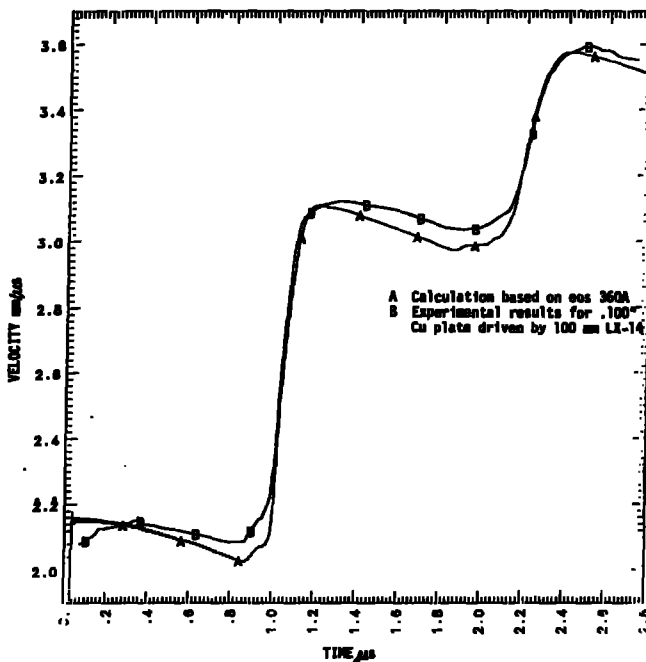


Fig. 13 Comparison of experimental and calculated initial motion histories.

ACKNOWLEDGMENT

We wish to acknowledge the considerable contributions of C. Pruneda, L. Meegan, and H. Chau to material preparation, test assembly, and Fabry Perot operation to the completion of this study.

REFERENCES

1. H. Jones and A. R. Miller, "The Detonation of Solid Explosives," Proc. Roy. Soc. London, A-194 480 (1948).
2. J. M. Walsh, M. H. Rice, R. G. McQueen, and F. L. Yarger, "Shock-Wave Compressions of Twenty-Seven Metals. Equations of State of Metals," Phys. Rev. 108, 196-216 (1957).
3. W. E. Deal, "Measurement of the Reflected Shock Hugoniot and Isentrope for Explosive Reaction Products," J. Chem. Phys. 27, 796 (1957).
4. E. L. Lee, H. C. Hornig, J. W. Kury, "Adiabatic Expansion of High Explosive Detonation Products," UCRL-50422, TID-4500, UC-4 Chemistry, Lawrence Radiation Laboratory, University of California, Livermore, CA, May 2, 1968.

5. W. A. Bailey, R. A. Belcher, D. K. Chilvers, G. Eden, "Explosive Equation of State Determination by the AWRE Method," Seventh Symposium (International) on Detonation, NSWC MP 82-334, Naval Surface Weapons Center, Annapolis, MD, June 16-19, 1981 VA
6. H. Chau, D. Goosman, J. Lyle, and M. Summers, "A Simple Velocity Interferometer System," Conference on Laser and Electro-optical Systems, OSA/IEEE, Abstract TUHH4, p. 20 (1978).
7. Tarver, C. et. al. *ibid* this Symposium
8. Deal, W. E., "Measurement of the Reflected Shock Hugoniot and Isentrope for Explosive Reaction Products," Phys. Fluids, Vol. 1 No. 6, 1958, p. 523-527.
9. Cast, J. C., Hornig, H. C., Kury, J. W., "Standard Test for Detonation Pressure Measurement," UCRL-50645, June 1969, Lawrence Livermore National Laboratory.